Targeted Inactivation of a Developmentally Regulated Neural Plectin Isoform (Plectin 1c) in Mice Leads to Reduced Motor Nerve Conduction Velocity*[S]

Peter Fuchs[‡1], **Michael Zörer**[‡1], **Siegfried Reipert**[‡], **Günther A. Rezniczek**[‡], **Friedrich Propst**[‡], **Gernot Walko**[‡], **Irmgard Fischer**[‡], **Jan Bauer**[§], **Michael W. Leschnik**[¶], **Bernhard Lüscher**[‖], **Johann G. Thalhammer**[¶], **Hans Lassmann**[§], **and Gerhard Wiche**[‡2]

From the ‡Department of Biochemistry and Cell Biology, Max F. Perutz Laboratories, University of Vienna, Dr. Bohr-Gasse 9, 1030 Vienna, Austria, the §Department of Neuroimmunology, Center for Brain Research, Medical University of Vienna, 1090 Vienna, Austria, the ¶Clinic for Internal Medicine and Infectious Diseases, University of Veterinary Medicine Vienna, 1210 Vienna, Austria, and the ‖Division of Biochemistry and Molecular Biology, Medical Faculty of the Rheinisch-Westfaelische Technische Hochschule Aachen University, 52074 Aachen, Germany

Cytolinker proteins stabilize cells mechanically, regulate cytoskeleton dynamics, and provide scaffolds for signaling molecules. For plectin, the prototype of these proteins, an unusual diversity of isoforms has been reported, which show distinct expression patterns, subcellular localizations, and functions. Plectin has been shown to have important functions in skin and muscle, but little is known about its role in neural cells. To address this issue, we generated two knock-out mouse lines, one which was selectively lacking plectin 1c (P1c), the major isoform expressed in neural cells, and another in which plectin was conditionally deleted in neuronal precursor cells. Using isoform-specific antibodies, we found P1c to be expressed late in development and to associate with postsynaptic dendrites of central nervous system neurons, motorneurons of spinal cord, sciatic nerve axons, and Schwann cells. Motor nerve conduction velocity was found significantly reduced in sciatic nerve from P1c-deficient as well as from conditional knock-out mice. This defect was traceable to an increased number of motor nerve fibers with small cross-sectional areas; the thicknesses of axons and of myelin sheaths were unaffected. This is the first report demonstrating an important role of plectin in a major nerve function.

Cytolinker proteins, like plectin, BPAG1, and ACF7/MACF1, are particularly abundant in tissues exposed to great mechanical stress, such as muscle and epithelia, and some of them show high level expression also in neural tissues. Besides contributing to tissue integrity, there is increasing evidence that cytolinker proteins play important roles as cytoplasmic scaffolding platforms for signaling cascades, controlling basic metabolic and dynamic activities of cells. The best studied example is plectin, which has been shown to regulate non-receptor tyrosine kinases, mitogen- and AMP-activated kinases, and protein kinase C (1–3).

With a few exceptions, our knowledge about cytolinker functions in neural cells of vertebrates is limited. Spontaneous deletions and targeted inactivation of *Bpag1* in mice cause dystonia musculorum, a neuropathy that manifests as a loss of motor activity caused by progressive degeneration of sensory neurons (4–6). In addition, the case of a 4-year-old patient, suffering from a defect in *Bpag1* and showing signs of non-progressive encephalopathy, severe motor and mental retardation, and delayed visual maturation, has been reported (7). ACF7/MACF1 is expressed in many regions of the brain (8), but since mice deficient in ACF7/MACF1 die early in embryonic development (9, 10), *in vivo* studies addressing its role in the central nervous system have not been reported. Early studies on plectin in the central nervous system of rats showed expression in brain and spinal cord gray and white matter cells, including ependymal cells, Bergmann glial processes, astrocytes, motorneurons, and endothelial cells (11). Similarly, in the central nervous system of humans, plectin was detected in capillary endothelial cells and astrocytes, and at pia/glia and endothelia/glia interfaces (12).

Plectin gene mutations lead to epidermolysis bullosa simplex (EBS)[3]-MD, EBS-Ogna, and EBS-PA, different forms of the disease EBS (reviewed in Ref. 13). For EBS-MD, the most common form of the disease, severe skin blistering, late onset muscular dystrophy, and in some cases cerebral and cerebellar atrophies were observed (14). Recently, plectin has also been implicated in Alexander disease, a rare neurological disorder caused by mutations in glial fibrillary acidic protein (GFAP) (15).

For plectin, an unusual diversity of isoforms has been reported (16, 17). Alternative splicing of a dozen different first

[S] The on-line version of this article (available at http://www.jbc.org) contains supplemental Figs. S1–S3.

[1] Both of these authors contributed equally to this work.

[2] To whom correspondence should be addressed: Dept. of Biochemistry and Cell Biology, Max F. Perutz Laboratories, University of Vienna, Dr-Bohr-Gasse 9, 1030 Vienna, Austria. Tel.: 431427752851; Fax: 431427752854; E-mail: gerhard.wiche@univie.ac.at.

[3] The abbreviations used are: EBS, epidermolysis bullosa simplex; GFAP, glial fibrillary acidic protein; P1c, plectin 1c; MNCV, motor nerve conduction velocity; *plec*[f/f], *plectin*[flox/flox]; GST, glutathione *S*-transferase; MBP, maltose-binding protein; IB, immunoblotting; IFM, immunofluorescence microscopy; A1c, anti-P1c antibodies; IEM, immunoelectron microscopy; IHC, immunohistochemistry; MAP, microtubule-associated protein; Ab, antibody; mAb, monoclonal antibody; NF, neurofilament; MTs, microtubules; EM, electron microscopy; WT, wild-type; P1c^{−/−}, P1c isoform-specific knockout; PBS, phosphate-buffered saline; PFA, paraformaldehyde.

exons into one common exon 2 gives rise to multiple variants differing only in relatively short N-terminal sequences. A number of recent reports show that these sequences confer specific functions to the distinct isoforms (18–22). The plectin isoform most prominently expressed in brain tissue is plectin 1c (P1c) (17). The diversity of P1c transcripts is further increased by three non-coding exons (−1, 0, and 0a) that are alternatively spliced into the first coding exon (1c). Additional plectin variants lacking the α-helical ~190-nm-long central rod domain of the protein (16) are expressed in the central nervous system, however only at a level that is ~20-fold lower than that of the full-length protein (23).

In the present study, we used P1c isoform-specific antibodies and generated P1c-deficient mice to address the following questions. (i) Is the expression of P1c in brain developmentally regulated? (ii) Is P1c compartmentalized within neural cells? (iii) Does P1c deficiency affect gross morphology and/or cytoarchitecture of neural cells? (iv) Can any neuropathological consequences of P1c deficiency be identified? In what follows, we provide answers to these questions and report as a key finding that P1c deficiency causes reduced motor nerve conduction velocity (MNCV) combined with a reduction in motor neuron calibers.

EXPERIMENTAL PROCEDURES

Gene Targeting—All experiments involving animals were performed in accordance with Austrian Federal Government laws and regulations. For generating P1c-deficient mice, a targeting construct was generated that enabled elimination of the DNA region harboring the alternative first coding exon 1c and the preceding non-coding exons 0, 0a, and −1 (supplemental Fig. S1A). This region was replaced by a neomycin resistance cassette flanked by two *loxP* sites. The targeting vector was constructed by joining a 5-kb fragment (flanked by XbaI and BamHI sites and located upstream of exon −1) and a 3.9-kb fragment (flanked by a NcoI and HindIII site and located downstream of exon 1c) to a thymidine kinase promoter-driven *neo* cassette (provided by M. Kraus, Institute for Genetics, University of Cologne, Cologne, Germany) in reverse transcriptional orientation (supplemental Fig. S1A). Using electroporation, the linearized targeting vector was introduced into ES cells. G418-resistant colonies were isolated (24), and clones with correctly targeted alleles were identified by Southern blot analysis. Germ line chimeras were bred to C57BL/6 females to obtain F1 mice heterozygous for the plectin 1 deletion. The sequence containing the neomycin resistance cassette was eliminated from the genome by interbreeding mice constitutively expressing Cre recombinase (Cre deleter strain (25)). The phenotypes of knock-out mice lacking or still containing the *neo* cassette were indistinguishable. The generation of *plectin$^{flox/flox}$* (*plec$^{f/f}$*) is described elsewhere (26). To increase the efficiency of Cre-mediated recombination, *plec$^{f/f}$* mice were first crossed with Cre deleter mice. The resulting *plec$^{f/\Delta}$* mice were then mated with mice overexpressing Cre under the control of the nestin promoter (*nes-Cre*) (27). RNase protection assays, including various exon-specific probes, have previously been described (17). Probes specific for exon 32 of mouse plectin and exon 5 of

Parp10 (poly(ADP-ribose) polymerase 10) were derived from genomic mouse λ clones preceding clone S1 (17).

Preparation of Teased Nerve Fibers—Sciatic nerves dissected from mice were fixed with 4% PFA in PBS for 30 min at room temperature. After washing with PBS, nerves were teased on gelatin chrome alum-coated glass slides and air-dried.

Generation of Anti-P1c (A1c) Antibodies—A mouse exon 1c BamHI/SalI cDNA fragment encoding amino acids 1–17 of P1c (GenBank^{TM} accession number NM_011117) was subcloned into vectors pGEX 4T-1 (GE Healthcare) or pMal-c2 (New England Biolabs) to obtain glutathione *S*-transferase (GST) and maltose-binding protein (MBP) fusion proteins, respectively. GST fusion proteins were purified on gluthathione-Sepharose 4B beads, as described in the manufacturer's instructions (GE Healthcare). MBP fusion proteins were solubilized in 20 mM Tris-HCl, pH 7.4, 200 mM NaCl, and 1 mM EGTA, and purified on amylose resin. 100 μg of GST-P1c fusion protein in 200 μl of PBS were mixed with 350 μl of either Freund's complete (for initial subcutaneous injections) or incomplete (for six booster injections at intervals of 4 weeks) adjuvant (Sigma). A1c antibodies were affinity-purified using Sepharose beads covalently linked to P1c-MBP fusion proteins. Eluted antibodies were stored frozen in 0.2 M Tris-HCl, pH 8.0, at a concentration equivalent to that in serum.

Immunoblotting (IB) and Immunofluorescence Microscopy (IFM)—To prepare brain and sciatic nerve tissue homogenates, tissues (600 mg) were mechanically disrupted, as described previously (28). After incubation with primary and horseradish peroxidase-conjugated secondary antibodies, blots were developed using SuperSignal substrate (Pierce).

Cultured cells and tissue sections of cortex, ependyma, and sciatic nerve tissues were processed for IFM, as described previously (26, 28). All processing steps were carried out at room temperature. Fixed cells and tissue sections were mounted in Mowiol (Hoechst) and viewed in a fluorescence laser-scanning microscope (LSM 510; Zeiss). Digital images were processed using Adobe Photoshop and Adobe Illustrator software.

Immunohistochemistry (IHC)—PFA-fixed spinal cords were dissected, postfixed with 4% PFA in PBS overnight, and embedded in paraffin. Sections (2 μm) were incubated with PBS, 10% fetal calf serum for 5 h, followed by incubation with primary antibodies for 72 h at 4 °C. Sections were then washed thoroughly with PBS, 10% fetal calf serum, followed by incubation with biotinylated secondary antibodies for 3 h, washing with PBS, 10% fetal calf serum, and incubation with avidin/peroxidase (Sigma) for 1 h (all steps at room temperature). Peroxidase conjugates were revealed using diaminobenzidine as chromogen, and counterstaining was performed with hematoxilin (Merck). Sections were dehydrated and mounted in Eukitt (Merck).

Histomorphometric Analysis—Phrenic nerve sections were toluidine blue-stained using the Unicryl staining kit (British Bio Cell) and viewed in an Axiophot microscope (Zeiss). For analyses of these samples, we developed a custom image processing software, where inner and outer borders of the myelin sheaths of individual axons are determined by evaluating contrast changes in images obtained from an Axiophot/Axiocam microscope system (Zeiss). Cross-sectional (inner) areas of axons

were determined by converting the number of pixels inside the myelin sheaths to metric area units. Myelin sheath thickness was measured by calculating the average distance between inner and outer borders, performing >300 measurements per axon across the full circle. All axons of several phrenic nerves were analyzed. Positions of NFs and microtubules (MTs) were marked in digital electron microscopy (EM) images of sections from L5 ventral roots. Coordinates of all filaments were determined, and nearest neighbor distances were calculated independently for all NFs and MTs. Filament densities were determined by applying a template of hexagons (each equivalent to an actual area of 0.1 μm^2) over each electron micrograph analyzed and counting the number of NFs and MTs within all hexagons.

Electrophysiology—MNCV was measured in sciatic nerves from mutant animals and their wild-type (WT) littermates. Animals were anesthetized with isoflurane/oxygen (2.5%) and placed on a water-circulated heating pad throughout the procedure. Nerves were supramaximally stimulated by percutaneous electrodes at the sciatic notch (34), and summation motor potentials were recorded by percutaneous electrodes at the metacarpus. The ground electrode was placed between stimulation and recording sites.

Electron Microscopy—For morphological and ultrastructural studies, tissues were fixed *in situ* by intracardial perfusion of adult mice with 2.5% PFA and 0.5% glutaraldehyde in PBS, pH 7.5, at 37 °C. Pieces of sciatic nerve were dissected and immersion-fixed with 3% glutaraldehyde in Sorensen's buffer at 4 °C overnight, followed by postfixation with 1.5% OsO_4, dehydration in ethanol, and embedding in epoxy resin (Agar 100; Gröpl). For immunoelectron microscopy (IEM), animals were perfused intracardially with 4% PFA in PBS. Brains were dissected and postfixed overnight in 4% PFA in PBS. Immunodetection was accomplished as described for spinal cords. Thin sections were cut using an Ultracut microtome (Leica Microsystems), contrasted with uranyl acetate and lead citrate, and viewed in a Jeol 1210 transmission electron microscope at 60 kV.

Antibodies—The following antibodies were used for IB, IFM, IEM, and IHC, under conditions as specified: A1c (IB, IFM, and IHC 1:500; IEM 1:1000), rabbit anti-pan-plectin antiserum (N-terminal) raised against a recombinant protein fragment of rat plectin corresponding to exons 9–12 (18) (IB 1:1500), rabbit anti-pan-plectin antiserum (number 46) (29) (IFM 1:200), rabbit anti-microtubule-associated protein 1B (MAP1B)-HC antiserum (30) (IB 1:1000), rabbit anti-Kv1.1 potassium channel antiserum (Alomone Laboratories) (IFM 1:50), rabbit anti-pan-sodium channel antiserum (Millipore) (IFM 1:20), rabbit anti-α-paranodin (L51) antiserum (31) (IFM 1:500), rabbit anti-α-Caspr2 (contactin-associated protein 2) (number 190) antiserum (32) (IFM 1:500), rabbit anti-neurofascin (NF155) antiserum (33) (IFM 1:1000), mouse monoclonal antibodies (mAbs) to neurofilament (NF) medium (NF-M) subunit protein (clone RMO44; Sigma) (IB 1:500), mAbs to α-tubulin (clone B-5-1-2; Sigma) (IB 1:1000), mAbs to synaptophysin (clone SY 38; DAKO) (IFM 1:20), mAbs to MAP2 (clone AP20; Roche Applied Science) (IFM 1:100), mAbs to GFAP (clone G-A-5; Roche Applied Science) (IFM 1:100), and mAbs to the three NF subunit proteins (clone 2F11; Dako) (IFM 1:100). As

secondary antibodies, we used horseradish peroxidase-conjugated goat anti-mouse (Jackson ImmunoResearch Laboratories) (IB 1:10,000), goat anti-rabbit (Bio-Rad) (IB 1:10,000), Texas Red-conjugated goat anti-rabbit (Jackson Immuno-Research Laboratories) (IFM 1:500), biotinylated goat anti-rabbit (Amersham Biosciences) (IHC 1:200), and Alexa Fluor 488-conjugated goat anti-mouse (Molecular Probes) (IFM 1:1000) IgGs.
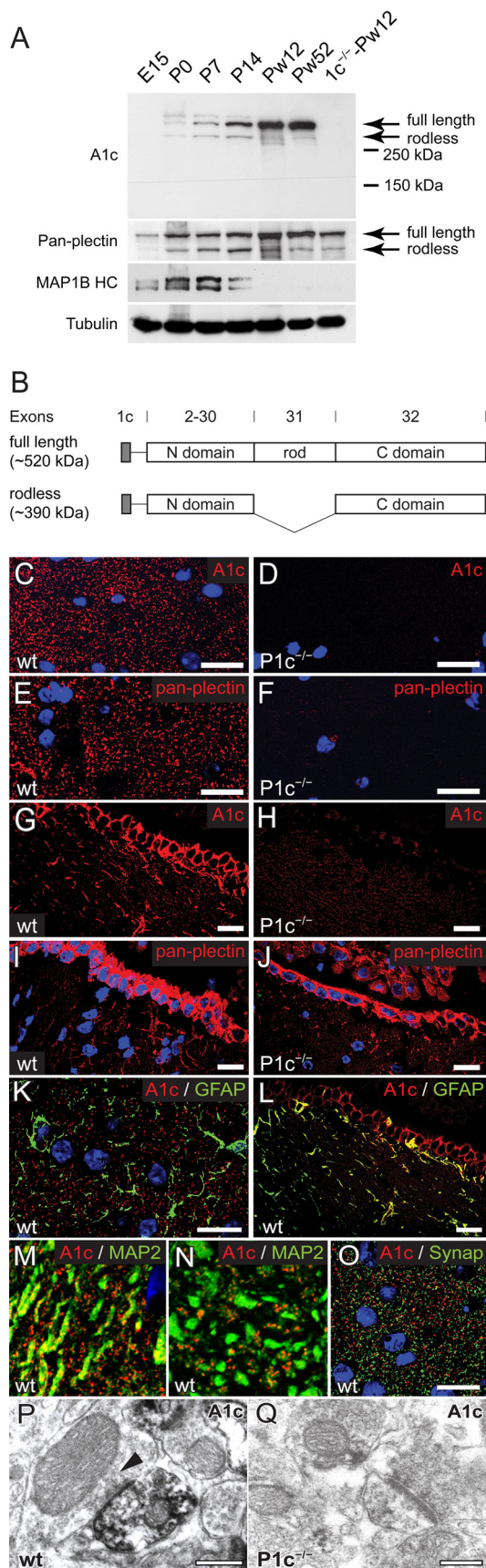
RESULTS

P1c, a Developmentally Late Expressed Isoform Is Widely Expressed throughout the Nervous System—The analysis of protein extracts from whole brains of mice at different developmental stages using isoform P1c-specific antibodies (A1c) revealed first emergence of P1c at birth, whereas other isoforms, detected with antibodies not discriminating between isoforms (pan-plectin), were present already at earlier stages (Fig. 1A). As previously shown for rat glioma C_6 cells, both A1c and pan-plectin antibodies detect full-length plectin as well as variants lacking the central rod domain (Fig. 1, A and B) (23). In juvenile mouse brain, we found relatively high expression levels of rodless P1c (390 kDa) compared with those of the full-length version (520 kDa), whereas in adult brain, the rodless form was detected at increasingly lower levels (Fig. 1A, A1c); a similar expression profile of rodless plectin versions was observed using pan-plectin antibodies (Fig. 1A).

To investigate the localization of P1c in neural tissue, frozen tissue and paraffin-embedded sections of various brain areas from adult mice were immunolabeled using A1c or pan-plectin antibodies. Corresponding samples from a P1c isoform-specific knock-out (P1c$^{-/-}$) mouse line (see below) served as negative controls. In the adult mouse brain, P1c was found in all gray matter areas. In the cerebral cortex, it was present in all cortical layers, with the strongest immunoreactivity being observed in the outer granular layer (data not shown). At higher magnifications, we observed a punctuate signal in cortical sections of WT (Fig. 1, C and E) but not P1c$^{-/-}$ mice (Fig. 1, D and F) with both antisera. In line with data reported for rat brain (11), a strong labeling of ependymal cells was detected using both antiserum A1c (Fig. 1G) and anti-pan-plectin antiserum (Fig. 1I). Whereas A1c staining was absent from P1c$^{-/-}$ mice (Fig. 1H), the residual staining of knock-out ependyma with anti-pan-plectin antiserum (Fig. 1J) indicated that isoforms other than P1c were additionally expressed in these cells.

IFM using antiserum A1c and antibodies to GFAP, showed that P1c was not present in cortical astrocytes (Fig. 1K), whereas astrocytes underneath the ependyma of the fourth ventricle were P1c-positive (Fig. 1L). Double labeling of P1c and the dendritic marker protein MAP2 revealed partially overlapping signals in samples where dendrites were cut longitudinally (Fig. 1M), suggesting expression of P1c in neuronal dendrites. In cross-cut dendrites, P1c/MAP2 colocalization was barely observed, albeit P1c- and MAP2-specific signals were found in close vicinity (Fig. 1N). A proximity of signals was also observed for P1c and synaptophysin (Fig. 1O). Such staining patterns were compatible with P1c being present in distal parts of dendrites that do not contain MAP2 (35). In fact, IEM of cerebral gray matter, using the immunoperoxidase technique, provided

unambiguous evidence that P1c resided in postsynaptic dendrites (Fig. 1, *P* and *Q*).
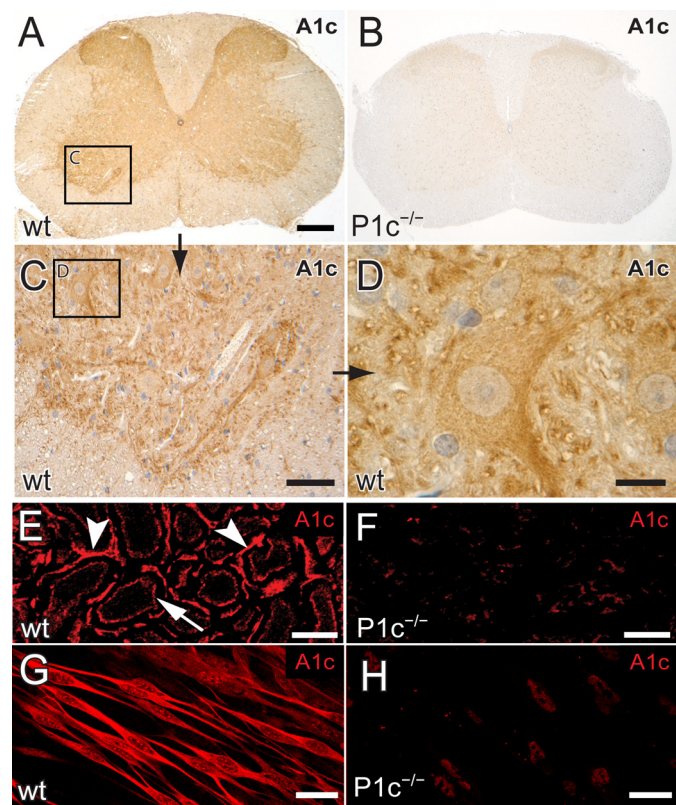
Immunohistochemistry on spinal cord sections of WT and P1c$^{-/-}$ mice (Fig. 2, *A* and *B*) revealed P1c expression mainly in the gray matter, in particular in motor neurons and smaller interneurons (Fig. 2, *C* and *D*). When frozen tissue sections of sciatic nerve were immunolabeled, P1c-specific signals were detected in peripheral areas of axons and in the cytoplasm of Schwann cells but not in myelin sheaths (Fig. 2, *E* and *F*). Strong expression of P1c could also be observed in primary cultures of Schwann cells obtained from sciatic nerves of 3–5-day-old WT mice (Fig. 2*G*); similar cultures from P1c$^{-/-}$ mice showed no specific staining (Fig. 2*H*). In both central nervous system and peripheral nervous system, P1c was expressed at relatively high levels, as revealed by immunoblotting of brain and sciatic nerve cell lysates (supplemental Fig. S1*E*).

Mice Lacking Plectin Isoform 1c Show Reduced MNCV—To uncover isoform-specific functions of P1c in neural cells against the background of all other isoforms, we generated a knock-out mouse line that specifically lacked this but no other isoform (for details, see supplemental Fig. S1). Addressing possible defects in peripheral nervous system functions, we measured the MNCV in sciatic nerves of anesthetized mice *in situ*. P1c$^{-/-}$ mice were found to have a significantly reduced conduction velocity compared with their WT littermates (27.25 ± 4.5 *versus* 52.32 ± 13.4 m/s; $p < 0.00001$) (Fig. 3*A*). In contrast, when sensory reflexes were assessed by measuring paw withdrawal thresholds after mechanical stimulation using von Frey fila-
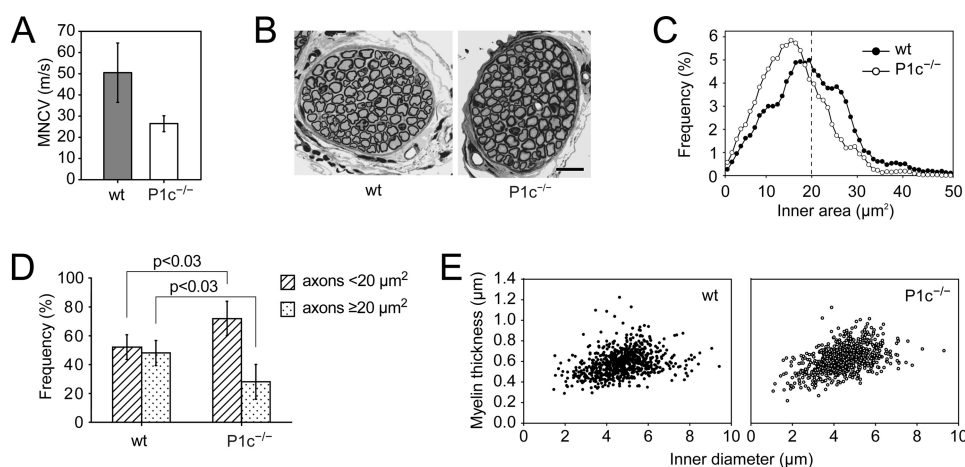
ies (Abs) used are indicated on the *left. MAP1B HC*, MAP1B heavy chain; *E15*, embryonal stage day 15; *P0, P7,* and *P14*, 0, 7, and 14 days after birth; *Pw12, Pw52,* and *1c$^{-/-}$-Pw12*, 12- and 52-week-old WT and 12-week-old P1c$^{-/-}$ mice, respectively. Tubulin served as loading control. Note that (i) A1c Abs label bands corresponding to full-length P1c (~520 kDa) and a rodless P1c variant (~390 kDa); (ii) pan-plectin (N-terminal) antibodies label bands corresponding to all full-length (~520 kDa) and rodless (~390 kDa) variants irrespective of their alternative first cooling exons (see also *B*); (iii) in adult mice (Pw12 and Pw52), rodless P1c is detectable only at low levels; and (iv) contrary to P1c, MAP1B is expressed at early developmental stages. *B*, schematic diagram of P1c protein variants. *Boxes* represent main domains of P1c. *Gray boxes*, amino acid sequence encoded by the alternative first exon 1c; *N domain*, N-terminal globular domain; *rod*, central coiled-coil rod domain; *C domain*, C-terminal globular domain of P1c. Exons coding for these domains are indicated. Alternative splicing events of different first exons into exon 2 are depicted by a straight line, the splice event leading to excision of exon 31 is indicated with a *kinked line*. The estimated molecular masses of full-length and rodless plectin variants are indicated. Note that A1c exclusively recognizes the exon 1c-encoded domain, whereas pan-plectin (N-terminal) recognizes epitopes in the N-terminal globular domain which is common to all plectin isoforms known so far. *C–F*, IFM of cortex sections from WT and P1c$^{-/-}$ animals using primary Abs as indicated. Note, Abs A1c and pan-plectin (number 46) both reveal punctuate staining patterns in WT but not P1c$^{-/-}$ cortex, establishing P1c as the dominating isoform in the cortex. Nuclei are stained with Hoechst dye. *G–J*, and *L*, IFM of fourth ventricle ependyma from WT and P1c$^{-/-}$ animals using primary Abs as indicated. Note (i) the residual staining of knock-out ependyma with anti-pan-plectin antiserum in *I* (indicating that isoforms other than P1c are additionally expressed in these cells) and (ii) P1c expression in ependymal cells and underlying astrocytes in *L*. *K* and *M–O*, IFM of WT cortex sections. Note that (i) punctuate P1c staining in *K* does not overlap with GFAP-positive astrocytes; (ii) the partial colocalization of P1c and MAP2 observed in longitudinally cut dendrites (*M*) is barely observed in cross-cut dendrites (*N*), where P1c- and MAP2-specific signals nevertheless are found in close vicinity to each other; and (iii) P1c is not localized in anti-synaptophysin (*Synap*)-immunostained presynaptic vesicles (*O*). *P* and *Q*, IEM of P1c-specific diaminobenzidine reaction product in WT (*P*) and P1c$^{-/-}$ (*Q*) cortex. Note the specific labeling of non-myelinated postsynaptic dendrites. *Arrowhead*, presynaptic vesicles. *Scale bars*, 25 μm (*G–J* and *L*), 20 μm (*C–F, K,* and *O*), 5 μm (*M* and *N*), and 0.3 μm (*P* and *Q*).

FIGURE 1. **Expression and subcellular localization of P1c in the central nervous system.** *A*, expression of P1c during brain development assessed by immunoblotting of brain homogenates from mice of different ages. Antibod-

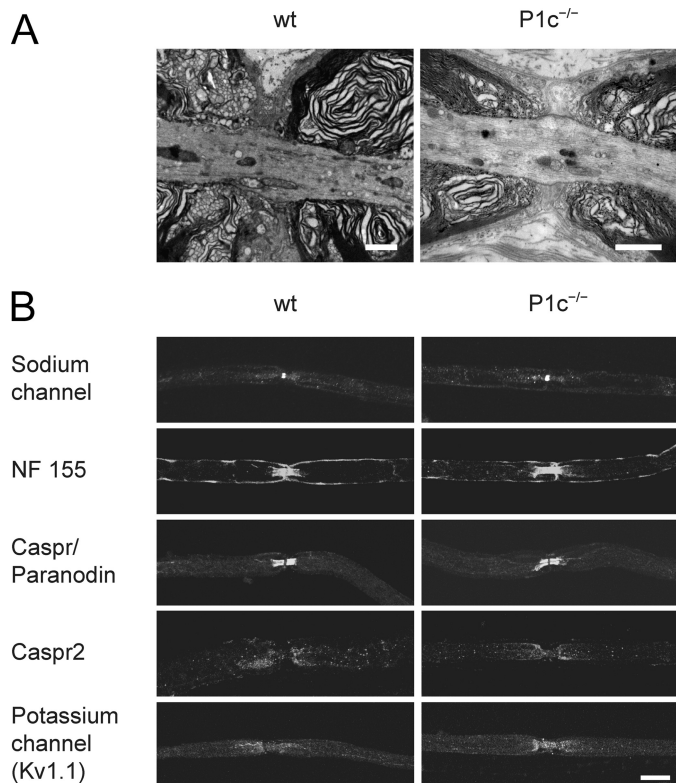# Nerve Conduction Velocity Is Plectin-dependent

FIGURE 2. **Expression of P1c in spinal cord and sciatic nerve.** *A–D*, immunohistochemistry (diaminobenzidine staining) of spinal cord sections. *Rectangles* marked in *A* and *C* are shown magnified in *C* and *D*, respectively. Note the prominent staining of WT gray matter in *A* and the positive staining of motor neurons and smaller interneurons in *C* and of the cell body and processes of a motor neuron in *D*. *E* and *F*, IFM of sciatic nerve cross-sections from WT (*E*) and P1c$^{-/-}$ mice (*F*) reveals strong A1c signals in Schwann cells (*arrowheads*) and relatively weak staining of axons (*arrow*). *G* and *H*, primary Schwann cells from WT (*G*) and P1c$^{-/-}$ mice (*H*). The weak nuclear staining in *F* and *H* is nonspecific. *Scale bars*, 200 μm (*A* and *B*), 50 μm (*C*), 20 μm (*G* and *H*), and 10 μm (*D–F*).

ments, in 10 independent assays (performed with 12 knock-out animals and their respective WT littermates), no differences were found (data not shown). To verify results obtained with P1c$^{-/-}$ mice, we also generated a nerve tissue-specific conditional plectin knock-out mouse line (*nes-Cre/plec$^{f/\Delta}$*) by crossing *plectin$^{flox/\Delta}$* mice (carrying one "floxed" and one plectin-null allele (26)) with mice (*nes-Cre*) expressing Cre recombinase under the control of the nestin promoter (27). Despite the highly efficient elimination of the floxed alleles in the central nervous system of *nes-Cre/plec$^{f/\Delta}$* mice, as shown by Southern blot analysis of genomic DNA isolated from the brain (supplemental Fig. S2*A*), immunolabeling of sciatic nerve cross sections revealed that just a fraction of the axons was devoid of plectin, whereas Schwann cells showed undiminished immunoreactivity (supplemental Fig. S2*C*). A quantitative analysis based on double labeling of 1842 sciatic nerve axons from three *nes-Cre/plec$^{f/\Delta}$* mice and their corresponding WT littermates with anti-plectin and anti-NF antibodies confirmed a complete abolishment of plectin expression in ~24% of the neurons (supplemental Fig. S2*C*). Although recombination had apparently taken place only in a fraction of the axons, MNCV again was found to be significantly lower in sciatic nerve from *nes-Cre/plec$^{f/\Delta}$* compared with control mice (30.8 ± 3.0 *versus* 42.0 ± 3.0 m/s; $p < 0.001$) (supplemental Fig. S2*D*). In fact, MNCVs measured in this case were very similar to those of P1c$^{-/-}$ mice (30.8 ± 3.0 and 26.5 ± 3.8 m/s, respectively).

Increased Number of Small Myelinated Axons in Peripheral P1c$^{-/-}$ Nerves—To correlate reduced MNCV with other phenotypic characteristica of P1c$^{-/-}$ mice, motor nerves of mutant and WT mice were subjected to ultrastructural and morphometric analyses. For these analyses, we used sciatic nerve, which contains both motor and sensory neurons, and phrenic nerve, consisting of a defined number (~260) of exclusively motor type neurons. In general, P1c-deficient axons did not show any obvious myelination defects or gross structural abnormalities. However, measuring the number, cross-sectional area, and myelin thickness of axons in an automated manner, using a newly developed computer-based method (see "Experimental Procedures"), we found phrenic nerves from knock-out animals to contain an altered proportion of small diameter *versus* large diameter axons. In particular, we observed a higher amount of axons with small cross-sectional areas ($<20 \mu$m^2; $p < 0.03$) and a lower amount of axons with large areas ($\geq 20 \mu$m^2; $p < 0.03$) in P1c$^{-/-}$, compared with WT mice (Fig. 3, *C* and *D*). Regarding nerve fiber morphology (Fig. 3*B*), numbers of axons (average of 263 and 243 for knock-out and WT mice, respectively), or thickness of myelin sheaths (Fig. 3*E*), no significant alterations were detectable. An

FIGURE 3. **Phenotypic analyses of P1c$^{-/-}$ mice.** *A*, MNCV measured in sciatic nerves of WT (*n* = 12) and P1c$^{-/-}$ mice (*n* = 12). Mean ± S.D. values are shown. *B*, toluidine blue-stained cross-sections of nervus phrenicus branches from WT and P1c$^{-/-}$ mice. *Scale bar*, 50 μm. *C*, distribution of cross-sectional (inner) areas of nervus phrenicus axons from WT and P1c$^{-/-}$ mice. Nerve preparations from five pairs of WT and knock-out littermates were analyzed (1215 and 1318 axons in total, respectively). Axons were sorted into clusters of 1-μm^2 width (0–1 μm^2, 1–2 μm^2, etc.), and frequencies were calculated for each cluster. Mean frequencies of four adjacent clusters are plotted *versus* inner area. *D*, numbers of axons $<20 \mu$m^2 (*hatched bars*) and $\geq 20 \mu$m^2 (*dotted bars*) in nervus phrenicus samples from WT and P1c$^{-/-}$ mice analyzed in *C*. The *dotted line* in *C* indicates the 20 μm^2 value. Mean ± S.D. values are shown. *E*, average thickness of myelin sheets from three pairs of WT and knock-out littermates (744 and 801 axons in total, respectively, were analyzed).

A

wt   P1c$^{-/-}$

B

wt   P1c$^{-/-}$

Sodium channel

NF 155

Caspr/ Paranodin

Caspr2

Potassium channel (Kv1.1)

FIGURE 4. **Analyses of nodes of Ranvier of WT and P1c$^{-/-}$ mice.** *A*, EM of ultrathin sections from WT and P1c$^{-/-}$ sciatic nerves showing nodes of Ranvier. *B*, localization of node of Ranvier proteins in WT and P1c$^{-/-}$ mice. IFM of teased sciatic nerve fibers from WT and P1c$^{-/-}$ mice using antibodies to the nodal sodium channels, the paranodal proteins neurofascin isoform 155 (NF155) and Caspr/paranodin, and the juxtaparanodal proteins Caspr2 and potassium channel subtype Kv1.1. *Scale bars*, 1 μm (*A*) and 10 μm (*B*).

ultrastructural examination of nodes of Ranvier from sciatic nerves of P1c$^{-/-}$ mice revealed no abnormalities in morphology, no unusual accumulation of cell organelles, and no obvious alteration in filament organization (Fig. 4*A*). Furthermore, proteins with established functions in different nodes of Ranvier compartments, including nodal sodium channels, the paranodal proteins neurofascin isoform 155 (NF155) and Caspr/paranodin, and the juxtaparanodal proteins Caspr2 and potassium channels subtype Kv1.1, showed unaltered localizations in P1c$^{-/-}$ mice (Fig. 4*B*).

Since plectin has been shown to bind to all three NF subunit proteins (36), and P1c, in particular, was found to colocalize with MTs in keratinocytes (18) and neural cells,[4] we examined whether P1c deficiency affected axonal interfilament spacing in L5 ventral roots of P1c$^{-/-}$ mice and their WT littermates by EM (Fig. 5*A*). Registering the positions of NFs and MTs and calculating nearest neighbor distances for each individual filament in axons of P1c$^{-/-}$ mice and WT littermates, we noticed a trend toward larger distances between NFs in P1c$^{-/-}$ axons, although statistically the difference was not significant (Fig. 5*B*). In the case of MTs, such a trend was not observed (Fig. 5*C*). When filament densities were directly measured by applying a template of hexagons over individual EM images and counting the numbers of NFs and MTs in each hexagon, the frequency

---

[4] G. Walko, I. Fischer, and G. Wiche, unpublished data.

distribution of NFs in mutant mice was slightly shifted toward hexagons containing fewer NFs (Fig. 5*D*), confirming the nearest neighbor analysis data; again, no differences were observed in the case of MTs (Fig. 5*E*).

DISCUSSION

Using isoform-specific antibodies, we found a polarized distribution of P1c to the postsynaptic dendritic cell compartment of non-myelinated central nervous system neurons. Since the P1c-specific staining pattern was indistinguishable from that observed with antibodies not discriminating between isoforms, and, moreover, since such antibodies were unreactive with dendrites of P1c$^{-/-}$ mice, we conclude that P1c is the only major plectin variant expressed in neurons of the central nervous system. This distinguishes central nervous system neurons from other cell types, such as keratinocytes and muscle fibers, where usually more than one variant of plectin is expressed (18, 21, 37). Similarly, in other types of central nervous system cells, such as ependymal cells and a subset of astrocytes, other (not yet identified) plectin isoforms were found to be expressed in addition to P1c.

Apart from plectin, two other plakin protein family members, BPAG1 and ACF7/MACF1, have been reported to be widely expressed in neuronal tissues (8, 38–40). BPAG1 has been localized in the cell body, dendrites, and axons of mature neurons and thus apparently does not exhibit a polarized distribution like P1c. In the case of ACF7/MACF1, transcripts were detected in cerebellum, hippocampus, and cerebral cortex, but very little is known about its subcellular localization. Hence, P1c is the only plakin protein family member known to date that specifically localizes to postsynaptic dendrites in the central nervous system. However, since alternative first exon-encoded N-terminal amino acid sequences of remarkable similarity to that of P1c exist for both BPAG1 and ACF7/MACF1 isoforms (17), it would not come as a surprise to us if eventually these proteins were found at similar locations.

Since P1c was detected in mouse brain only at late developmental stages, its expression profile would fit with the growing number of synapses developing in the brain of young animals. One may therefore speculate that P1c could play a role in the formation of synapses and/or maintenance of their functional integrity. The novel mouse models described here could be useful tools for future studies addressing these questions in more detail.

Since we found P1c to be abundantly expressed in peripheral nerve cell axons and in their associated myelinating Schwann cells, a role in peripheral neural cell function, such as in nerve conduction, was not unexpected. Two independent knock-out strategies, the isoform-specific knock-out and the neuronal cell-restricted (nestin-Cre-mediated) conditional knock-out, both led to animals with reduced MNCV. It was important to confirm the phenotype observed in the plectin isoform-deficient mouse line in an alternative system, because a recent analysis of the genomic locus upstream of the plectin gene revealed that two of its non-coding exons (−1 and 0a), which directly precede exon 1c, were also part of transcripts encoding PARP10, a newly identified member of the PARP protein family (41) (supplemental Fig. S3*A*). As a consequence of this exon
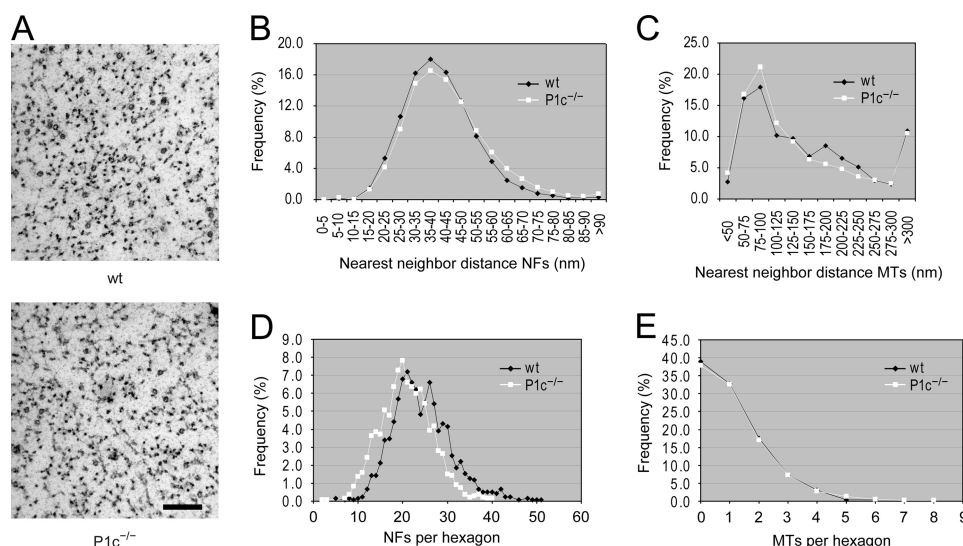
FIGURE 5. **Ultrastructural analysis of L5 ventral roots of P1c$^{-/-}$ mice and their WT littermates.** *A*, EM of cross-sectioned L5 ventral root motor axons from WT and P1c$^{-/-}$ mice. *Scale bar*, 200 nm. *B* and *C*, nearest neighbor analyses of NF (*B*) and MT (*C*) spacing in WT and P1c$^{-/-}$ mice. Preparations of L5 ventral roots from three pairs of WT and P1c$^{-/-}$ littermates were analyzed (in total 41 and 32 axons, respectively). *D* and *E*, NF (*D*) and MT (*E*) densities in WT and P1c$^{-/-}$ mice. A template of hexagons was applied over each electron micrograph analyzed, and the number of NFs and MTs was counted in all hexagons ($n = 1180$, WT; $n = 1380$, P1c$^{-/-}$).

sharing, the P1c$^{-/-}$ mouse line that we have generated represents in fact a double knock-out (P1c$^{-/-}$/PARP10$^{-/-}$). Whereas PARP10 transcripts were not detectable in the central nervous system, they were found to be expressed in sciatic nerve to some extent (supplemental Fig. S3, *B* and *C*). Hence, theoretically the lack of PARP10, and not that of P1c, could have been responsible for the observed phenotype of reduced MNCV in P1c$^{-/-}$ mice. However, this possibility can be ruled out, because the conditional *nes-Cre/plec$^{f/\Delta}$* mouse model (where plectin was knocked down, leaving PARP10 unaffected) showed a similar MNCV reduction.

The only other plectin-related cytolinker for which gene mutations leading to defects in peripheral nerve function have been reported is BPAG1. In one of several mouse lines carrying the mutation dystonia musculorum (42), the missing exons in the *Bpag1* locus encode an N-terminal BPAG1 sequence, which is quite similar to a corresponding one in plectin. However, contrary to dystonia musculorum mice, which show progressive degeneration of sensory neurons, loss of motor activity, myelination abnormalities (caused by defects in the function of Schwann cell), and axonal swellings (5, 39, 43), the phenotypic alterations of P1c$^{-/-}$ mice were restricted to reduced MNCV and a shift of axon diameters toward smaller calibers.

Interestingly, the phenotypes more closely resembling those of P1c$^{-/-}$ mice turned out to be the ones of mice with deficiencies in proteins falling into the category of plectin binding partners. For instance, axonal atrophy along with reduced MNCV have been reported for MAP1B-null mice (30), suggesting a role of MAPs in peripheral nerve axon caliber determination, reminiscent of P1c. Whereas MAP1B knock-out mice displayed abnormal brain architecture, including delayed myelination and tract malformation (30, 44), mice deficient for another plectin interaction partner, MAP2 (45), showed a less severe phenotype, manifesting as subtle alterations in axonal cytoarchitecture (46). Reduced MNCVs have also been observed in

knock-out mouse models lacking one of the three NF subunit proteins, L, M, or H (47, 48), all of which have been shown to bind to plectin (36). Although no myelination defects were detectable in any of these mice, in all of them axon diameters were found shifted toward smaller calibers, and in NF-L- and NF-M-deficient mice, additionally, axonal loss was observed (47, 48). Thus, among all of these knock-out lines, the phenotype of NF-H-null mice was the one most closely resembling that of the P1c$^{-/-}$ mice.

Two explanations were offered for the NF-H-null phenotype: (i) that axonal caliber reduction is the sole reason for diminished MNCV (48), and (ii) that a putative NF-H-dependent effect influences the clustering and/or function of potassium channels (47). In motor neurons lacking P1c, we did not detect any dislocation of key proteins present at nodes of Ranvier, such as juxtaparanodal potassium channels and Caspr2, paranodal proteins Caspr/paranodin and NF155, or nodal sodium channels; nor did nodes of Ranvier show any structural abnormalities, nor were nodal distances altered. Consequently, for P1c$^{-/-}$ mice, a relatively small shift of axon calibers toward smaller diameters may be the main reason for reduced MNCV. Nevertheless, despite being properly located, cation channels could still be functionally affected by P1c deficiency. In a recent study, spectrins (αII and βII) and ankyrin B were found to be part of a specialized paranodal cytoskeleton (49). Since plectin was shown to interact with spectrins (45), its absence from peripheral nerve axons could destabilize this cytoskeletal system and therefore affect axonal membranes and/or ion channel properties.

In summary, by using isoform-deficient as well as nerve tissue-specific conditional plectin knock-out mice, we uncovered a specific function of a plectin isoform (P1c) in motor neuron performance. A reduction of conduction velocity in sciatic nerve could be traced to reduced axon calibers. On the other hand, P1c seems not to be essential for brain and peripheral nervous system development. The molecular mechanisms leading to axon caliber changes remain to be elucidated, including open questions of whether P1c influences cytoskeleton dynamics and/or ion channel functions. The new mutant mouse lines described here may become useful also for behavior and cognition studies addressing the role of P1c in the central nervous system.

REFERENCES

1. Osmanagic-Myers, S., and Wiche, G. (2004) *J. Biol. Chem.* **279,** 18701–18710
2. Osmanagic-Myers, S., Gregor, M., Walko, G., Burgstaller, G., Reipert, S., and Wiche, G. (2006) *J. Cell Biol.* **174,** 557–568
3. Gregor, M., Zeöld, A., Oehler, S., Marobela, K. A., Fuchs, P., Weigel, G., Hardie, D. G., and Wiche, G. (2006) *J. Cell Sci.* **119,** 1864–1875
4. Guo, L., Degenstein, L., Dowling, J., Yu, Q. C., Wollmann, R., Perman, B., and Fuchs, E. (1995) *Cell* **81,** 233–243
5. Bernier, G., De Repentigny, Y., Mathieu, M., David, S., and Kothary, R. (1998) *Development* **125,** 2135–2148
6. Bernier, G., and Kothary, R. (1998) *Dev. Genet.* **22,** 160–168
7. Giorda, R., Cerritello, A., Bonaglia, M. C., Bova, S., Lanzi, G., Repetti, E., Giglio, S., Baschirotto, C., Pramparo, T., Avolio, L., Bragheri, R., Maraschio, P., and Zuffardi, O. (2004) *J. Med. Genet.* **41,** e71
8. Bernier, G., Pool, M., Kilcup, M., Alfoldi, J., De Repentigny, Y., and Kothary, R. (2000) *Dev. Dyn.* **219,** 216–225
9. Kodama, A., Karakesisoglou, I., Wong, E., Vaezi, A., and Fuchs, E. (2003) *Cell* **115,** 343–354
10. Chen, H. J., Lin, C. M., Lin, C. S., Perez-Olle, R., Leung, C. L., and Liem, R. K. (2006) *Genes Dev.* **20,** 1933–1945
11. Errante, L. D., Wiche, G., and Shaw, G. (1994) *J. Neurosci. Res.* **37,** 515–528
12. Lie, A. A., Schröder, R., Blümcke, I., Magin, T. M., Wiestler, O. D., and Elger, C. E. (1998) *Acta Neuropathol.* **96,** 215–221
13. Pfendner, E., Rouan, F., and Uitto, J. (2005) *Exp. Dermatol.* **14,** 241–249
14. Smith, F. J., Eady, R. A., Leigh, I. M., McMillan, J. R., Rugg, E. L., Kelsell, D. P., Bryant, S. P., Spurr, N. K., Geddes, J. F., Kirtschig, G., Milana, G., de Bono, A. G., Owaribe, K., Wiche, G., Pulkkinen, L., Uitto, J., McLean, W. H., and Lane, E. B. (1996) *Nat. Genet.* **13,** 450–457
15. Tian, R., Gregor, M., Wiche, G., and Goldman, J. E. (2006) *Am. J. Pathol.* **168,** 888–897
16. Elliott, C. E., Becker, B., Oehler, S., Castañón, M. J., Hauptmann, R., and Wiche, G. (1997) *Genomics* **42,** 115–125
17. Fuchs, P., Zörer, M., Rezniczek, G. A., Spazierer, D., Oehler, S., Castañón, M. J., Hauptmann, R., and Wiche, G. (1999) *Hum. Mol. Genet.* **8,** 2461–2472
18. Andrä, K., Kornacker, I., Jörgl, A., Zörer, M., Spazierer, D., Fuchs, P., Fischer, I., and Wiche, G. (2003) *J. Invest. Dermatol.* **120,** 189–197
19. Rezniczek, G. A., Abrahamsberg, C., Fuchs, P., Spazierer, D., and Wiche, G. (2003) *Hum. Mol. Genet.* **12,** 3181–3194
20. Abrahamsberg, C., Fuchs, P., Osmanagic-Myers, S., Fischer, I., Propst, F., Elbe-Bürger, A., and Wiche, G. (2005) *Proc. Natl. Acad. Sci. U.S.A.* **102,** 18449–18454
21. Konieczny, P., Fuchs, P., Reipert, S., Kunz, W. S., Zeöld, A., Fischer, I., Paulin, D., Schröder, R., and Wiche, G. (2008) *J. Cell Biol.* **181,** 667–681
22. Winter, L., Abrahamsberg, C., and Wiche, G. (2008) *J. Cell Biol.* **181,** 903–911
23. Fuchs, P., Spazierer, D., and Wiche, G. (2005) *Cell Mol. Neurobiol.* **25,** 1141–1150
24. Hogan, B., Beddington, R., Constantini, F., and Lacy, E. (1994) *Manipulating the Mouse Embryo: A Laboratory Manual*, Cold Spring Harbor Laboratory, Cold Spring Harbor, NY
25. Schwenk, F., Baron, U., and Rajewsky, K. (1995) *Nucleic Acids Res.* **23,** 5080–5081
26. Ackerl, R., Walko, G., Fuchs, P., Fischer, I., Schmuth, M., and Wiche, G. (2007) *J. Cell Sci.* **120,** 2435–2443
27. Tronche, F., Kellendonk, C., Kretz, O., Gass, P., Anlag, K., Orban, P. C., Bock, R., Klein, R., and Schütz, G. (1999) *Nat. Genet.* **23,** 99–103
28. Rezniczek, G. A., Janda, L., and Wiche, G. (2004) *Methods Cell Biol.* **78,** 721–755
29. Wiche, G., and Baker, M. A. (1982) *Exp. Cell Res.* **138,** 15–29
30. Meixner, A., Haverkamp, S., Wässle, H., Führer, S., Thalhammer, J., Kropf, N., Bittner, R. E., Lassmann, H., Wiche, G., and Propst, F. (2000) *J. Cell Biol.* **151,** 1169–1178
31. Peles, E., Nativ, M., Lustig, M., Grumet, M., Schilling, J., Martinez, R., Plowman, G. D., and Schlessinger, J. (1997) *EMBO J.* **16,** 978–988
32. Denisenko-Nehrbass, N., Oguievetskaia, K., Goutebroze, L., Galvez, T., Yamakawa, H., Ohara, O., Carnaud, M., and Girault, J. A. (2003) *Eur. J. Neurosci.* **17,** 411–416
33. Tait, S., Gunn-Moore, F., Collinson, J. M., Huang, J., Lubetzki, C., Pedraza, L., Sherman, D. L., Colman, D. R., and Brophy, P. J. (2000) *J. Cell Biol.* **150,** 657–666
34. Waikar, S. S., Thalhammer, J. G., Raymond, S. A., Huang, J. H., Chang, D. S., and Strichartz, G. R. (1996) *Brain Res.* **721,** 91–100
35. Bernhardt, R., and Matus, A. (1984) *J. Comp. Neurol.* **226,** 203–221
36. Foisner, R., Leichtfried, F. E., Herrmann, H., Small, J. V., Lawson, D., and Wiche, G. (1988) *J. Cell Biol.* **106,** 723–733
37. Rezniczek, G. A., Konieczny, P., Nikolic, B., Reipert, S., Schneller, D., Abrahamsberg, C., Davies, K. E., Winder, S. J., and Wiche, G. (2007) *J. Cell Biol.* **176,** 965–977
38. Yang, Y., Dowling, J., Yu, Q. C., Kouklis, P., Cleveland, D. W., and Fuchs, E. (1996) *Cell* **86,** 655–665
39. Dowling, J., Yang, Y., Wollmann, R., Reichardt, L. F., and Fuchs, E. (1997) *Dev. Biol.* **187,** 131–142
40. Dalpe, G., Leclerc, N., Vallee, A., Messer, A., Mathieu, M., De Repentigny, Y., and Kothary, R. (1998) *Mol. Cell Neurosci.* **10,** 243–257
41. Lesniewicz, K., Lüscher-Firzlaff, J., Poreba, E., Fuchs, P., Walsemann, G., Wiche, G., and Lüscher, B. (2005) *Genomics* **86,** 38–46
42. Duchen, L. W. (1976) *Adv. Neurol.* **14,** 353–365
43. Bernier, G., Brown, A., Dalpé, G., De Repentigny, Y., Mathieu, M., and Kothary, R. (1995) *Mol. Cell Neurosci.* **6,** 509–520
44. Takei, Y., Kondo, S., Harada, A., Inomata, S., Noda, T., and Hirokawa, N. (1997) *J. Cell Biol.* **137,** 1615–1626
45. Herrmann, H., and Wiche, G. (1987) *J. Biol. Chem.* **262,** 1320–1325
46. Teng, J., Takei, Y., Harada, A., Nakata, T., Chen, J., and Hirokawa, N. (2001) *J. Cell Biol.* **155,** 65–76
47. Kriz, J., Zhu, Q., Julien, J. P., and Padjen, A. L. (2000) *Brain Res.* **885,** 32–44
48. Rao, M. V., Garcia, M. L., Miyazaki, Y., Gotow, T., Yuan, A., Mattina, S., Ward, C. M., Calcutt, N. A., Uchiyama, Y., Nixon, R. A., and Cleveland, D. W. (2002) *J. Cell Biol.* **158,** 681–693
49. Ogawa, Y., Schafer, D. P., Horresh, I., Bar, V., Hales, K., Yang, Y., Susuki, K., Peles, E., Stankewich, M. C., and Rasband, M. N. (2006) *J. Neurosci.* **26,** 5230–5239